Int J CARS (2010) 5 (Suppl 1):S122–S130
DOI 10.1007/s11548-010-0446-3

Treating Disease in the Abdomen: Can Registered Image Guidance Assist the Gastroenterologist and Abdominal Surgeon?*

K.G. Vosburgh[1,b], R. San José Estépar[2]
[1]Brigham and Women's Hospital, CIMIT, Boston, MA, United States
[2]Brigham and Women's Hospital, Harvard Medical School, Boston, MA, United States
*Supported by the Center for Integration of Medicine and Innovative Technology (CIMIT) and the National Cancer Institute under award R42 CA115112-03 and the National Center for Image Guided Therapy under award U41 RR019703.

Keywords Image-guided therapy · Surgery · Endoscopy · Laparoscopy

Purpose

Technology improvements have enabled image-guided procedures throughout the body, as methods pioneered in neurosurgery may now be implemented more broadly [1]. These include: observation of the therapeutic target, analysis of the target extent and the best path for therapeutic access, sensing the position of instruments and anatomic movement, monitoring the effects of therapy, and, finally, controlling the therapeutic process [2]. The anatomic coverage, speed, and quality of radiologic images have improved continuously, so that procedures conducted within or adjacent to imaging equipment can now more effectively show changes in the state of the patient, and thus provide direct, useful feedback to the physician. Here, we explore providing this "image-registered" insight to the physician using an endoscope or laparoscope outside the radiology suite to, in a similar fashion, better enable navigation and therapeutic performance.

Methods

Table 1 describes the necessary functional blocks; they are analogous to those for "in scanner" approaches, but some technical specifications and other requirements differ.

Results

These technical goals have been achieved at four sites in porcine [3] and human subject tests. A workstation (Windows XP platform, 3D Slicer User Interface) is coupled to a "flat plate" transmitter/sensor system supplied by Ascension Technologies Corp.; the sensors are placed at the tip of an instrument to measure its position in the body. The entire "open architecture" system is built with commercial components costing, in total, less than $10,000; it appears that it will be easily operated by clinical personnel with minimal training. Standard CT DICOM files are used for model creation, although image segmentation, at present, requires an experienced operator.

A guided laparoscopic ultrasound examination of the retroperitoneal space of a human patient was made James Ellsmere, MD in Halifax, NS to plan surgical resection of a tumor on the stomach wall (Fig. 1). The goal was to locate the superior mesenteric artery, which had been displaced by the tumor. Five human subjects with pancreatic disease were examined using image-registered gastroscopic ultrasound (IRGUS) at Brigham and Women's Hospital by Christopher Thompson, MD (Fig. 2). It was found that the system permits the operator to maintain acoustic contact easily, thus simplifying and reducing the time of the examination. For all patients, we observed a good correlation of pancreas features (stones, cysts, etc.) between

Table 1 Characteristics of System Elements for Image Registered Procedures

System Element and Function	Key Factors
Segmentation. Working from a 3D volumetric examination created by MR or CT, distinguish key anatomic features and build a solid model of the patient showing those features.	• Semi-automatic, with minimal trained supervision required; eventually fully automatic • Model features are appropriate to the particular interventional task
Tracking. Provide direct digital information on the spatial location of key elements, such as interventional instruments and, sometimes, the patient.	• Fast (no lag at video rates) • Stable (no jitter) • Adequate volume • Minimal interference with the procedure • Capable of being sterilized, easily
Registration. Align the patient, the segmented model, and the instrument tracking system so that information from these three sources are geometrically synchronized	• Sufficiently accurate (<5mm) • Stable • Minimal impact on procedure set-up time • Compatible with the procedure environment (particularly sterility)
Display. Present the model, tracked elements, and image data to the physician operator	• Real time, lag free (30 fps) • Easily understood • Solid, extensible software platform • High fidelity display

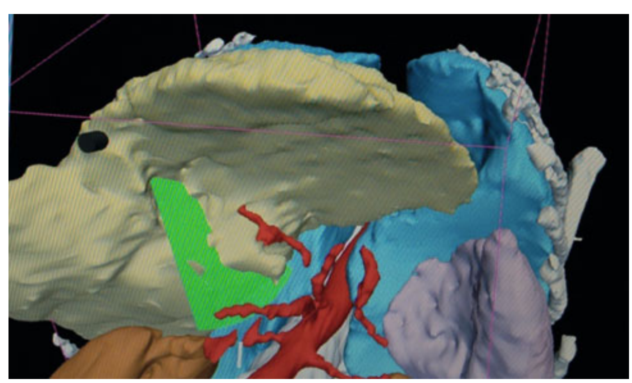

Fig. 1 Image registered laparoscopic ultrasound in a human patient: the ultrasound image plane (in green) is slicing through the liver, showing the location of a major artery (red). The major branching vessels off the aorta are easily displayed

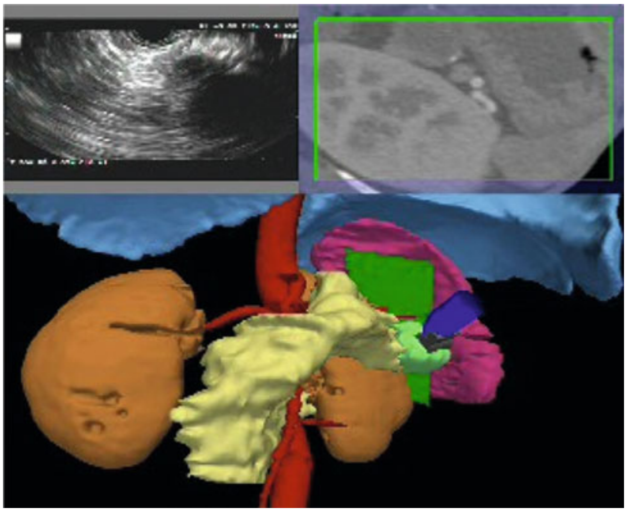

Fig. 2 Image registered endoscopic ultrasound in a human patient: Top Left: B-Scan Ultrasound Image. Top right: Image Reformatted CT Data in US-Defined Plane. Bottom: 3D CT-Based Model of Patient for Navigation and Biopsy Probe Positioning. The pancreas is yellow, the ultrasound image plane is green, the kidneys are orange

ultrasound and reformatted CT. Some other organs (such as the liver) did not align well, since they were shifted by gravity, due to left lateral decubitus patient positioning.

Conclusions

A low cost, easily adopted system to improve the performance of endoscopic and laparoscopic interventions has been developed and tested in animal models and human subjects. Operators found the system useful for navigation and for maintaining ultrasound contact. Studies continue at the two active clinical sites to validate these advantages by comparing with conventional procedures. These approaches appear to be extensible to other applications, and particularly to improve the accuracy and safety of a variety of "freehand" procedures. The low cost and intuitive operation of the system appear to offer significant advantages which will promote its adoption.

References

[1] Peters, T, K. Cleary, (eds.) Image-Guided Interventions: Technology and Applications. Springer 2008, New York.

[2] Vosburgh, K.G., Jolesz, F.A., The Concept of Image-Guided Therapy, Acad. Radiol. 2003;10:176–179.

[3] Vosburgh, KG. N. Stylopoulos, R. San José Estépar, R. E. Ellis, E. Samset, and C. C. Thompson. EUS and CT improve efficiency and structure identification over conventional EUS. Gastro. Endoscopy 2007 65(6):866–870.

Respiratory motion control for computer-assisted liver interventions: Accuracy of temporary tubus disconnection

G. Widmann[1], P. Schullian[1], H. Marion[1], F. Wiedermann[2], R. Bale[1]

[1]Medical University of Innsbruck, Department of Radiology, Innsbruck, Austria

[2]Medical University of Innsbruck, Department of Anaesthesiology, Innsbruck, Austria

Keywords Interventional radiology · Respiratory motion control · Temporary tubus disconnection · Accuracy · Liver intervention

Purpose

Precise application of computer-assisted guidance technology such as 3D-navigation, stereotaxy, and robotics for interventions in the liver is only achievable when the imaged body region is a stationary volume unaffected by patient movements, arm position, and liver motion secondary to respiration. Therefore, patient immobilisation and control of respiratory motion are substantial tasks before clinical implementation of these novel technologies. Purpose was to clinically assess respiratory motion control for stereotactic liver targeting in anaesthesized patients by temporary tubus disconnection as a modified standardized breath-hold technique.

Methods

The study has been approved by the Institutional Review Board and informed consent was obtained from all patients. The study protocol included patients from the period of October 2008 to October 2009 who had radiofrequency ablation of liver tumors based on interventional planning CTs in both, arterial and portal phase.

After general anaesthesia and muscle relaxation, patients were immobilized on the CT table via the BodyFix vacuum cushion system (Medical Intelligence GesmbH, Schwabmünchen, Germany).

Respiratory motion control was based on temporary disconnections of the endotracheal tubus. The procedure was executed and controlled by the attending anaesthesist in the intervention room.

Prior to imaging, 10-15 artificial skin markers (Beekley SPOTS®, Beekley Corporation, Bristol, CT, USA) were broadly placed around the thorax/upper abdomen. Contrast enhanced planning CTs (Siemens SOMATOM Sensation Open, Siemes AG, Munich, Germany) in 3 mm slice thickness were performed in both, arterial and portal phase (90-120 ml Iodixanol 320 mg J/mg, 3ml/sec) during the same phase of tubus disconnection. The native control CT in 3 mm slice thickness after electrode positioning was performed during a second phase of tubus disconnection. Before targeting, the treatment area has been disinfected and draped by a translucent plastic foil that included a self tapping field at the target area.

The respiratory motion control error (RMCE) was evaluated by subtracting the Euclidean error (distance of two points in space) of corresponding artificial skin markers = external targets and anatomic landmarks = internal targets during two phases of tubus disconnection (contrast enhanced arterial planning CT and native control CT) with the Euclidean error of the same points during the same phase of tubus disconnection (contrast enhanced arterial and portal planning CT).

The CT scans were fused using the ImMerge^{TM} fusion software (Medtronic Inc., Louisville, USA). In each CT scan, 5 external targets and 5 internal targets were identified. Only anatomic landmarks that were clearly identifiable in all CT images were chosen. Examples included diversion of the celiac trunc into the propria hepatic artery and the left gastric artery, diversion of the right hepatic artery, diversion of the portal vein, and (if available) radiopaque landmarks such as surgical clips and calcifications.

Data analysis and descriptive statistics were performed using PASW Statistics 17.0 (SPSS Inc., Chicago, Illinois, USA). Quantitative data were described with mean values, standard deviation and range.

One-way ANOVA and Student T-Test were used to determine significant statistical differences between the groups. Post hoc analysis was performed by the Bonferroni adjustment (for homogene variances) and by the Dunnett T3 test (for nonhomogene variances). A p-value less than .05 was defined as statistically significant.

Results

In 26 patients, the Euclidean error of a total of 520 targets was subdivided into four groups of 130 targets each, correlating to the Euclidean error of external and internal targets during the first tubus disconnection (reflecting the fusion error) and to same targets after the second tubus disconnection and insertion of intervention needles (reflecting the fusion error + respiratory motion control + draping + electrode insertion).

The mean Euclidean error during the same phase of tubus disconnection was .39 ± .31 mm (range 0 - 1.4 mm) for the external targets and .71± .50 mm (range .1 - 3.8 mm) for the internal targets. The mean Euclidean error during the two phases of tubus disconnection was 2.37 ± 1.31 mm (range .2 - 6.2 mm) of external targets and 2.12 ± 1.12 mm (range .4 - 5.6 mm) of internal targets.

Statistical group analysis showed significant differences between all groups except for internal vs. external targets between two phases of tubus disconnection (p-value .453).

The mean respiratory motion control error (RMCE) for external targets was 1.98 mm ± .93 mm (range .44 - 4.02 mm) and 1.41 ± .75 mm (range .46 - 3.18 mm) for the internal targets. As an implication of the evaluation method, RMCE included shift errors by draping and electrode insertion. Statistical analysis of the RMCE between internal and external targets yielded no significant difference in means (p-value .558).

The temporary interruption of air supply was well tolerated by the patients and did not produce any noticed complications during or after anaesthesia.

Conclusion

As evaluated under clinical conditions, respiratory motion may be accurately controlled by temporary disconnections of the endotracheal tubus in patients under general anaesthesia. The technique may represent a valuable means for respiratory motion control in 3D-navigated, stereotactic, or robotic interventions in the liver.

Image detection tracking of subsurface structures in laparoscopy

D. Kwartowitz[1], D. Holmes[1], A. Mariani[2], P. Weavers[3], R. Robb[1]
[1]Mayo Clinic, Biomedical Imaging Resource, Rochester, MN, United States
[2]Mayo Clinic, Gynecologic Surgery, Rochester, MN, United States
[3]Mayo Clinic, Department of Physiology and Biomedical Engineering, Rochester, MN, United States

Keywords Image-guided surgery · Laparoscopy · Real-time imaging · Image processing

Purpose

The use of image-guidance in medical procedures continues to increase as new applications are developed and current techniques are improved. One of the primary benefits of image-guidance is to locate sub-surface structures that may not be visible otherwise. These sub-surface structures may be critical for resection or may pose risks if violated.

In gynecologic surgery, ureteral injury is a fairly important complication, leading to post surgical complications ranging from pain to kidney necrosis. It is common practice in open surgery for the surgeon to locate the ureter at the beginning of the case and mark it such that its position is known. This process is difficult to perform in laparoscopic surgery because of the limited field of view and continually changing frames of reference due to camera movements.

We have examined the use of a CCD camera system in a series of mock surgical experiments in developing a novel method of subsurface structure localization and tracking.

Methods

In order to localize and track the position of any subsurface structure, the object must be made visible to an imaging modality that can be tracked within the same coordinate space as the laparoscopic camera. To maintain orientation as well as reduce the amount of additional equipment required for the procedure, a chemoluminescent tracer was chosen that would be visible to the currently used laparoscopic camera.

In order to choose an optimal chemoluminecent marker, first the camera system had to be analyzed for color response and sensitivity.

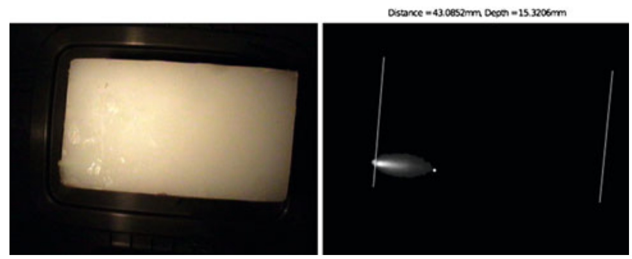

Fig. 1 (**a**) Illuminated frame from tissue penetration phantom. Chemoluminescent agent is illuminated however not visible. (**b**) Illustration of the segmented chemoluminescent agent within the tissue phantom. The vertical lines represent the edges of the phantom segmented through manual methods. The white dot is the point at which the penetration depth was measured

This was accomplished through gamut analysis of the camera's response to light of known brightness. An ideal chemoluminescent agent is detectable by the camera system, but is not visible under normal lighted conditions.

To test camera color response we obtained primary color samples red, blue, and green. These samples were illuminated to known illumination levels. These levels were measured at each test using a reflective ambient light meter. The camera's response to each color, as well as white was examined and compared to a standard digital camera with known gamut.

Chemoluminescent agent was then placed into a phantom made of dragon skin (Smooth-On, Easton, PA, USA) with a known internal gradient of depth. Green, blue, red, and pink samples of the agent were measured. A series of samples were taken with the scene illuminated with external lighting, and then a series of frames were taken with the external illumination off. The frames with the illumination off were integrated to improve the signal to noise ratio.

Finally, to test this method in respect to natural tissue, the chemoluminescent agent was placed into a sample of animal fat. The fat was heated to body temperature in an oven to render it comparable to living tissue. The experiment was repeated with illumination and dark scenes.

Results

The method has demonstrated to be simple and accurate in locating subsurface structures using equipment surgeons are already accustomed to using. The analysis of camera response demonstrated a bias towards the red end of the spectrum. Use of red dyes however is non-optimal due to the natural coloration of surrounding tissues.

Using a green chemoluminscent agent the depth of penetration was shown repeatedly to be 1.5 cm through dragon skin (Fig. 1). The chemolumiscent agent was also shown to penetrate through the animal fat to be visible.

Conclusions

Localization of subsurface structures during surgery is essential for avoidance of surgical injury or complication. Current methods of localization of subsurface structures in laparoscopic surgery require repeated anatomic identification, which is time consuming. The method presented here has demonstrated excellent penetration in both phantom and ex vivo tissue. Refinement of this method by integration with tracking and preoperative imaging should allow for reduction of repeated attempts to localize the ureter during gynecologic surgery. Extension to other organs and structures is possible.

Automated detection and display of abdominal lymph nodes from CT volumes based on local intensity structure analysis

K. Mori[1], Y. Nakamura[2], T. Kitasaka[3], M. Ito[4], S. Nawano[5], M. Kazunari[6], F. Michitaka[7]
[1]Nagoya University, Information Planning Office, Nagoya, Japan
[2]Nagoya University, Graduate School of Information Science, Nagoya, Japan
[3]Aichi Institute of Technology, Faculty of Information Science, Toyota, Japan
[4]National Cancer Center Hospital East, Kashiwa, Japan
[5]International University of Health and Welfare Mita Hospital, Tokyo, Japan
[6]Aichi Cancer Center Hospital, Nagoya, Japan
[7]Nagoya University, Graduate School of Medicine, Nagoya, Japan

Keywords Lymph node · Segmentation · Surgical planning · CAD · CT

Purpose

This paper presents a method for detecting abdominal lymph nodes from contrasted CT volumes and displaying them for endoscopic surgery assistance. As one of minimum-invasive surgical procedures, laparoscopic surgery is widely performed. Since the field view of the laparoscope and the operable area of the forceps are very limited, it is very important to make a surgical plan before actual surgery. For such surgical planning, information that can be obtained from CT volumes plays very important role. In such planning, a surgeon needs to check abdominal blood vessel network, variation of branching pattern of vessels, or locations of lymph nodes. Information of inflammatory lymph node location is very important in determination of resection area, since resection area should be optimum for preventing re-occurrence of cancer or deterioration of quality of life. If we could automatically extract lymph nodes from CT volume and display them in 3D views, it would be helpful to determine resection area or surgical procedure to be performed.

Lymph nodes show spherical or elliptical shape on CT images. Local intensity structure of a lymph node shows blob-like structure (CT values becomes high from peripheral to center.) There are several reports on automated extraction of abdominal lymph nodes by finding objects of such shape. The previous method extracted lymph nodes from contrasted CT volumes by employing a second-order directional difference filter called Min-DD. The Min-DD filter outputs high values for spherical objects. Although this method is sensitive to isolated (solitary) lymph nodes existing in a fat region, it overlooked lymph nodes existing close to the primary focus or attaching to other organs. However, these lymph nodes still show blob-like intensity structure. It would be possible to detect lymph nodes of isolated or close to primary focus by utilizing a filter enhancing blob-like structure.

In this paper, we propose an automated method to extract abdominal lymph nodes based on local intensity structure analysis for enabling to detect lymph nodes overlooked in the previous method. Candidate regions are extracted by blob structure enhancement filter followed by the classification process. The detection process target the lymph node of 5mm in diameter or above.

Methods

1. Automated detection process consists of four steps: (a) enhancement of blob-like region, (b) region growing, (c) FP reduction using information of normal structure, and (d) FP reduction based on feature analysis.
2. Enhancement of blob-like region

We emphasize blob-like regions by using eigenvalues of a Hessian matrix. We apply a Gaussian filter of standard deviation s to an input CT volumetric image and obtain the smoothed image $\mathbf{G}^s$. A Hessian matrix H for each voxel $\mathbf{p}$ of the smoothed image is computed by performing curve fitting of local intensity and calculation of partial derivatives of the fit curve. We compute three eigenvalues λ_1, λ_2, λ_3 ($\lambda_1 > \lambda_2 > \lambda_3$) and corresponding eigenvectors $\mathbf{e}_1$, $\mathbf{e}_2$, and $\mathbf{e}_3$. Blob-like regions are enhanced by

$$\mathrm{B(p)} = |\lambda_1|(\lambda_2/\lambda_3)(\lambda_1/\lambda_2) \text{ for } \lambda_3 \le \lambda_2 \le \lambda_1 < 0,$$
$$= 0 \text{ for otherwise.}$$

For enabling to detect lymph nodes of different sizes, we compute $\mathbf{B}$ ($\mathbf{p}$) for each voxel with different scale s (controlling standard deviation of Gaussian filter and the local size of curve fitting) and perform scale-integration. The enhanced image $\mathbf{M(p)}$ is obtained by

$$\mathrm{M(p)} = \max_s(\alpha_s \, \mathrm{B}_s(\mathrm{p})),$$

where α_s is a parameter for controlling scale-integration. The initial candidate regions are obtained by thresholding $\mathbf{M(p)}$ with threshold T.

3. Region growing

We perform region growing process by using each voxel of candidate regions as seed points of the growing process. The growing is performed if a target voxel $\mathbf{p}$' satisfies $|\mathbf{G}^1(\mathbf{p}') - \mathbf{G}^1(\mathbf{p})| \le 50$ [H.U.] where $\mathbf{p}$ means a seed point and $\mathbf{G}^1(\mathbf{p})$ gives the intensity value at the voxel $\mathbf{p}$ of the image smoothed by the smallest scale. The growing area is limited within the spherical region whose diameter is equal to the scale s selected for the voxel p in the scale-integration process.

4. FP reduction using normal structure

Lymph node candidate regions obtained in the previous step include many bone regions or fecal inside the colon. We eliminate such regions by the following process. First, we extract high CT value regions as bone regions. Also low CT value regions are extracted as air or fecal regions. Lymph node candidate regions are removed if they overlap with high or low CT value regions.

5. FP reduction based on feature analysis

We remove FPs by analyzing features of each connected component of candidate regions. The features utilized here include two types of features: (a) shape feature and (b) intensity feature. The shape features are (1) ratio of volume and surface area, (2) spherical rate of inscribed sphere and (3) spherical rate of circumscribed sphere. The intensity features are (1) average CT value in a connected component, (2) minimum CT value, (3) maximum CT value, (4) median of CT values, (5) first quartile of CT values inside a connected component, (6) third quartile of CT values. The mean vectors and covariance matrices are calculated for TP and FP categories. The quadratic classifier is utilized for distinguish each candidate regions is TP candidate or FP candidate.

6. 3D display of lymph node

We generate 3D display of lymph nodes detected by the proposed method. To assist a surgeon, lymph node regions are displayed with blood vessel network of the abdomen. Also, the locations of lymph nodes can be overlaid on the virtual laparoscopic views that can be synchronized with a real laparoscopic image.

Results

We applied the proposed method to five cases of contrasted 3D images. Acquisition parameters of CT images are: 512 × 512 × 401 - 451 voxels, 0.586 × 0.576 × 1.0 [mm^3] voxel sizes. We utilized three scales s = 1.0 [mm], 2.0 [mm], 3.0 [mm]. Example of lymph node detection and ROC curve is shown in Fig. 1 and 3D display of lymph nodes and arteries are shown in Fig. 2. Experimental result showed that the proposed method can detect lymph nodes with 79.2% sensitivity and 98 FPs, while the previous method showed 55.7% sensitivity and 57 FPs (operation points are indicated by arrows on the ROC curves). The proposed method can improve sensitivity of lymph node detection without explosive increase of FPs. Small lymph nodes overlooked by the previous method can be identified by the proposed method. Since the proposed method can detect small lymph node that is often overlooked by a surgeon, it is quite useful to make surgical plan that determines resection area. Three-dimensional display of lymph nodes assist a surgeon to understand the locations of lymph nodes in the pre- or intra-operative stages. Although the proposed method produces 98 FPs, these are very easy to be distinguished by a surgeon. Since the system is aimed for to be utilized for surgical

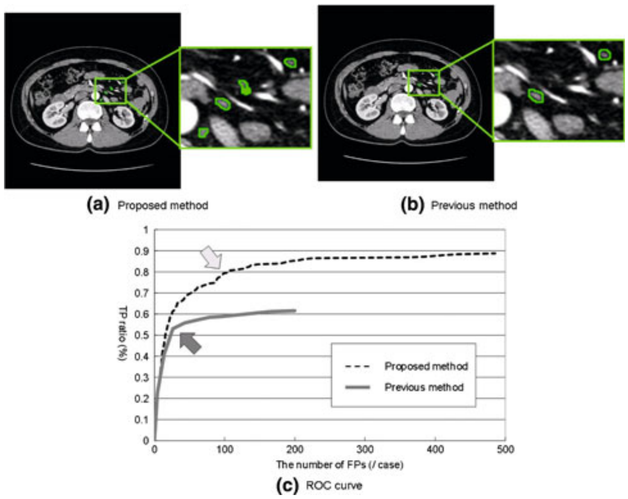

Fig. 1 Example of lymph node detection and ROC curve. (**a**) TP detection by proposed method. and (**b**) by previous method, and (**c**) ROC curve. Detected lymph nodes are contoured by green lines. Proposed method can successfully detect lymph nodes that are missed by previous method. ROC curve shows proposed method has good performance

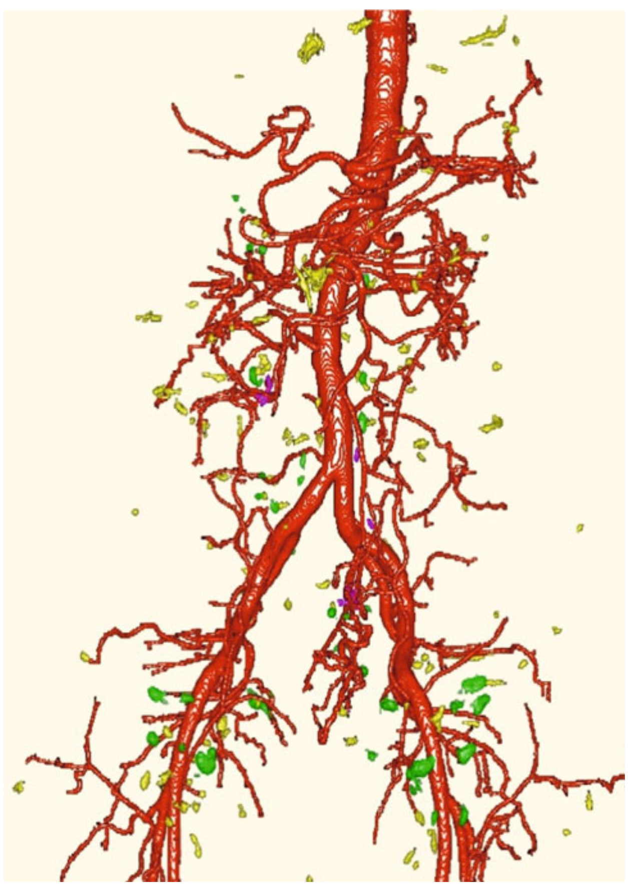

Fig. 2 3D Display of lymph node automatically detected and arteries.TP, FP and FN regions are colored in green, yellow and pink, respectively

assistance, it is much important to detect small lymph nodes that can be easily overlooked. Though further reduction of FPs and improvement of TPs are needed, the results of the current system are promising.

Conclusion

We presented a method for detecting abdominal lymph nodes from contrasted CT volumes and displaying them for endoscopic surgery assistance. The experimental results showed that the proposed method can detect lymph node region by 79.2%.

A proposal for laparoscopic cholecystectomy planning based on a simulated camera

J.L. Moyano Garcia-Cuevas, F.M. Sánchez Margallo, J.B. Pagador Carrasco, J.A. Sánchez Margallo, L.F. Sáchez Peralta, C. Illana Alejandro, M.F. Valdivieso, J.U. Gargallo
Minimally Invasive Surgery Centre Jesus Uson, Caceres, Spain

Keywords Planning · Navigation · Laparoscopic · Cholecystectomy · Camera

Purpose

Cholecystectomy is one most common intervention in laparoscopic surgery. This intervention presents several complications for patient's safety. In this paper, we present a system for planning this intervention from images acquired from CT and MRI. This system allows surgeons to visualize the abdominal cavity with a simulated laparoscopic camera. Afterwards, a comparison between the simulated camera and the real one is established.

Methods

Pigs and corpses have been used in this study to develop and validate the system. The liver was scanned by MRI and CT in operative position. Abdominal wall deformation and laparoscopic navigation are the main contributions of the proposed system. It allows the simulation of the abdominal wall deformation by the recreation of the space produced by the pneumoperitoneum. The validation of the system has been focused on the behaviour of the simulated laparoscopic camera. The field of view of the simulated camera and one of the real camera have been compared.

Results

A mean distance of 89.6 ± 0.58 mm was obtained for the real camera and 89.7 ± 0.6 mm for the simulated one. No significant differences between both fields of views were obtained after carrying out tests based on real images of different animals ($p < 0.05$).

Conclusion

The navigation of the system works properly. This result together with previous works lead us to the conclusion that the proposed system in this work can help surgeons to plan the cholecystectomy interventions as it allows identifying anatomical structures and complications that could appear.

Mixed reality for laparoscopic distal pancreatic resection

F. Volonte[1], P. Bucher[1], F. Pugin[1], A. Carecchio[1], M. Sugimoto[2], O. Ratib[3], P. Morel[1]
[1]HUG, Visceral and Transplantation Surgery, Geneva, Switzerland
[2]Kobe University Graduate School of Medicine, Gastroenterology, Kobe, Switzerland
[3]HUG, Department of Radiology and Medical Informatics, Geneva, Switzerland

Keywords Mixed reality · Overlay navigation surgery · OsiriX · Laparoscopic surgery

Purpose

Laparoscopic distal pancreatectomy may be a challenging procedure because of the inability for the surgeon to touch nodules hidden in the pancreatic tissue. These are often invisible on the surface of the organ.

Moreover, the anatomy of the area, with the splenic vessels that line the pancreas, spleen and digestive structures, requires extra care because a major local bleeding would quickly perturb the laparoscopic technique.

Methods

Superimposing 3D reconstructions made from simple slices of CT scan with a beamer, we brought in the operating room a new tool that increased perception of the surgeon in the operative field showing structures not detectable by the simple laparoscopic vision.

Our patient has a small nodule in the tail of the pancreas with a PET CT hot spot on the surface of the right colon, not visible at colonoscopy, possibly a tumor implant. A resection of the nodule on the right colon with frozen section and resection of the tail of the pancreas was decided. For a precise localization, the two lesions were plotted with different colors on the CT images and therefore safely isolated on 3D reconstructions (Fig. 1). This was possible with open source software OsiriX, developed by Rosset and Heuberger, whose use is possible even for physician not specialist in radiology. These images were then projected on the patient himself with a beamer fixed to the operating table. This technique of augmented reality enabled us to accurately locate anatomical landmarks on the surface of the patient and plan the lesions resection (Fig. 2). The instruments for the intervention have been placed with greater reliability knowing exactly where the lesions were located (Fig. 3). The three-dimensional image was also displayed on a large screen positioned at the left of the usual laparoscopy screen.

Results

The nodule on the surface of the right flank was resected in the middle of the fatty tissue overlying the colon thanks to the directives given by the superposition of reconstructed images. The frozen section confirmed the presence of a nodule with fibrous and inflammatory response without signs of malignancy. The pancreatic nodule was then clearly identified through the superimposed images and anatomy displayed on the large screen. The splenic vessels also have been spared because of their easier spatial identification.

Conclusion

Augmented reality, namely the overlay of virtual images on the real world is a valuable aid in interventions that are increasingly conducted in laparoscopic way or with the help of a robot. These techniques, which allow us to be less invasive and significantly reduce postoperative morbidity, have the disadvantage of removing the operator from the operating field, by interposing a mechanical instrument or a digital interface between the pathologic structure and the surgeon's touch. We must therefore find the system to replace the operator's sense of touch. Overlaying 3D images on the patient himself in order to accurately locate these structures and to display the same images beside the laparoscopic video gives the surgeon a new perception of the operating field and a real advantage compared to simple laparoscopy. This technique substitute to the lack of sense of touch that is proper to the laparoscopic technique.

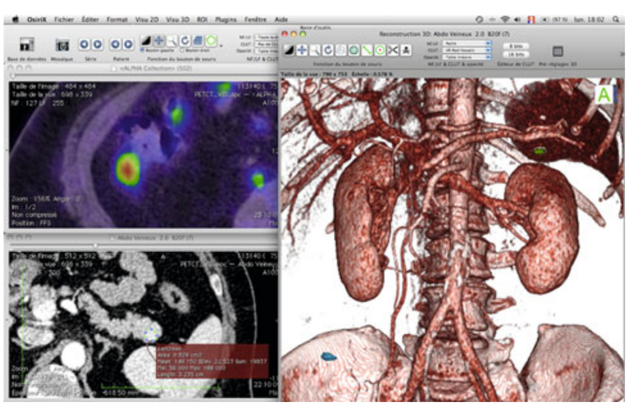

Fig. 1 Lesions plotted with different colors on CT slices and showed on 3D reconstructions

Fig. 2 Augmented reality – superimposition of 3D reconstructions on patient surface

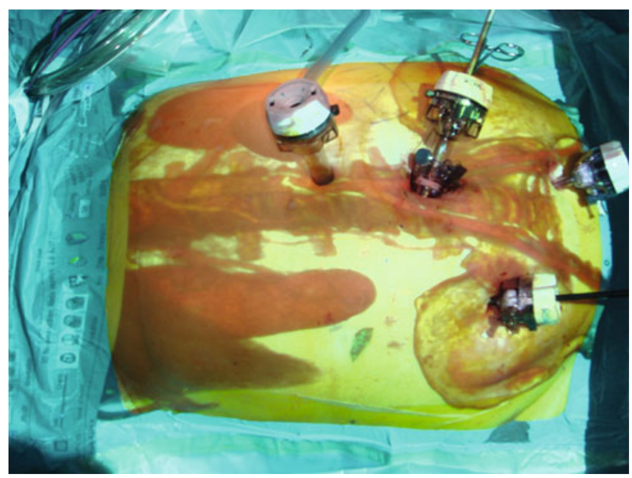

Fig. 3 Placement of ports based on the superimposition of normal anatomy and lesions

A new Concept for Ultrasound Imaging during laparoscopic Tumor Resection in Urology

J. Gumprecht[1], T. Maier[1], M. Markert[1], J.-U. Stolzenburg[2], T.C. Lüth[1]

[1]Technische Universität München, MiMed, Garching, Germany

[2]Universitätsklinikum Leipzig, Klinik und Poliklinik für Urologie, Leipzig, Germany

Keywords Ultrasound · Laparoscopy · Urology · Imaging

Purpose

Cancer of urogenital organs is one the most frequent reasons of death caused by cancer in Germany [1]. Laparoscopic resection of these tumors has become more and more popular since almost every urologic operation can be performed laparoscopically just as efficiently, and with fewer and less serious complications, as with conventional open surgery [2].

Observation of the target area via a laparoscope is the gold standard of intraoperative imaging in laparoscopic surgery. However, laparoscopes allow only for monitoring of the organ's surface. Therefore, it is impossible to detect the boundaries of a tumor within an organ as well as internal blood vessels intraoperatively. This can lead to a positive tumor margin, to a spread of tumor cells, or to an avoidable high blood loss during the resection of cancer.

Ultrasonography is an intraoperative imaging modality that provides an internal view of the target organ. Laparoscopic, rectal, and transcutaneous ultrasound transducers are commercially available but have rarely been used during laparoscopic interventions due to the following reasons: Laparoscopic ultrasound transducers require an additional but not available working channel to be applied simultaneously during the use of laparoscopic instruments. The operation range of rectal ultrasonography is very limited. Transcutaneous ultrasonography provides a detailed overview of the target area but can not be applied through the pneumoperitoneum (gas in the abdomen).

Transcutaneous ultrasound through the back of a supine patient could overcome this obstacle but has not been established in the clinical routine yet. We hypothesize that it is possible to build an apparatus that allows for transcutaneous ultrasonography of a patient lying on the back.

In a first step, we constructed an evaluation model to answer the following questions: What material can be used for the surface on which the patient rests? How can the built-in ultrasound transducer be moved? What medium can be used to guide the ultrasound waves from the transducer to the contact surface? What sterilization concept is applicable?

Methods

The patient rest mock-up consists of an aluminium tank that is covered with a flexible silicone membrane of 1mm thickness and shore 40A (Siltec GmbH & Co.KG, Weiler-Simmerberg, Germany) (Fig. 1). We designed and installed a customized one dimensional rail system in the tank and attached a commercial ultrasound probe (Teratech, Burlington, MA, USA) to it. The transducer has an operation frequency of 7.5MHz and a penetration depth of 90mm. It can be moved manually from outside via a shaft that pierces through the wall of the tank. The tank is filled with water to transmit the ultrasound waves from the transducer to the membrane. The difference in the acoustic impedance between the water and the membrane is sufficient to couple ultrasound waves in the silicone foil. Before the application, the membrane of the rest has to be greased with ultrasound transmission gel to permit the coupling of ultrasound waves into the body of the patient. Furthermore, the whole device must be wrapped up in sterile foil to guarantee for sterility of the rest. The operation position is at the lower back of the patient. This area must be greased with ultrasound gel as well.

We performed two experiments to determine whether the patient rest fulfils the set requirements. First, we assessed its stability i.e. if it is able to hold the weight of the patient. Therefore, we increased the pressure in the tank in steps of 0.05bar until it started to leak. Second, we measured the accuracy of the ultrasound images generated by the transducer in the tank. Therefore, we placed an ultrasound phantom on the membrane and recorded the ultrasound images of the phantom. In the phantom there were wires clamped with a diameter of 0.2mm and a distance of 10mm. To assess the accuracy we compared the distance of ten wires in the ultrasound images with the built-in metric scale of the manufacturer's software. Additionally, we measured the width and the height of the wires in the images.

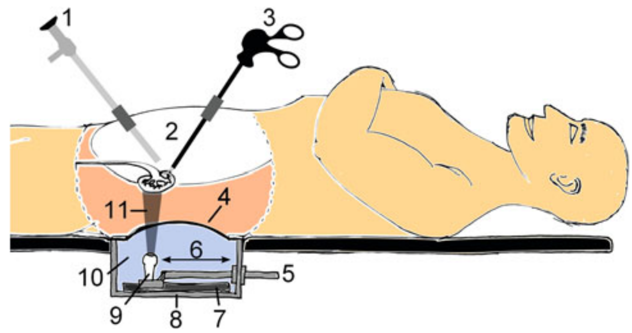

Fig. 1 1: Laparoscope, 2: Pneumoperitoneum 3: Laparoscopic instrument, 4: Flexible membrane, 5: Shaft to move the transducer, 6: Directions of movement of the ultrasound transducer, 7: Customized rail system to move the transducer 8: Tank, 9: Ultrasound transducer, 10: Water to guide the ultrasound waves from the transducer to the membrane, 11: Fan of ultrasound waves

Results

The tank could hold a pressure of up to 0.1bar which corresponds to a maximum load of 3750kg. Eight distances between different wires were measured (Fig. 2). The mean measured distance between two wires was 10.4mm $\pm$ 0.2mm (SD). The average width of the wires in the images was 0.3mm $\pm$ 0.1mm (SD) and the average height 0.6mm $\pm$ 0.1mm (SD).

Conclusion

In this paper we describe a new concept for ultrasound imaging during laparoscopic tumor resection in urology. We built a mock-up patient rest with a manually movable built-in transcutaneous ultrasound transducer to answer initial questions.

The study shows that the transition of the ultrasound waves through the water and the silicone membrane does not affect the accuracy of the ultrasound image. Thus, the image quality is only limited by the ultrasound device. Furthermore, the rest is stable enough to hold the weight of the patient. Sterility is guaranteed through the covering with a sterile foil.

Future steps will introduce more degrees of freedom for the movement of the ultrasound transducer as well as an automatic actuation of the kinematics.

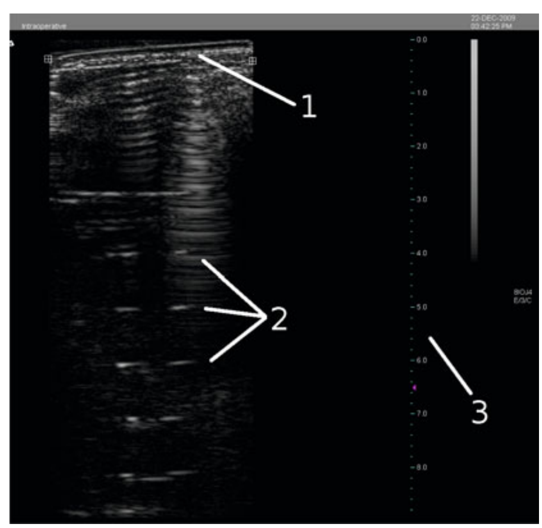

Fig. 2 1: Front face of the phantom; 2: Wires in the phantom; 3: Metric scale

We would like to thank the DFG for founding this research project through the Grant LU 604/27-1.

References

[1] Batzler, W.U.; Giersiepen, K.; Hentschel, S.; Husmann, G.; Kaatsch, P.; Katalinic, A.; Kieschke, J.; Kraywinkel, K.; Meyer, M.; Stabenow, R.; Stegmaier, C.; Bertz, J.; Haberland, J. and Wolf, U. (2008) Krebs in Deutschland, 6.überarbeitete, aktualisierte Ausgabe, Gesellschaft der epidemiologischen Krebsregister in Deutschland e.V. und das RKI, Saarbrücken.

[2] Stolzenburg, J.U.; Gettman, M.T. and Liatsikos, E.V. (2007) Endoscopic Extraperitoneal Radical Prostatectomy, Springer, Heidelberg.

Multi-DOF forceps for robot-assisted pediatric laparoscopic surgery

M. Fujii[1], K. Fukushima[1], N. Sugita[1], T. Ishimaru[2], T. Iwanaka[2], M. Mitsuishi[1]

[1]The University of Tokyo, School of Engineering, Tokyo, Japan

[2]The University of Tokyo Hospital, Department of Pediatric Surgery, Tokyo, Japan

Keywords Laparoscopic surgery · Multi-DOF forceps · Master-Slave robotic system · Pediatric surgery

Purpose

The objective of our research is to develop a master-slave robotic system for pediatric laparoscopic surgery. As the first step, we develop a multi-DOF forceps for pediatric laparoscopic surgery. Pediatric laparoscopic surgery has two problems. Firstly, multidirectional suture using the conventional forceps is difficult because it has lower maneuverability. Secondly, the existing multi-DOF forceps cannot be applied to pediatric laparoscopic surgery due to its size. To resolve these problems, we propose a new mechanism for the forceps which has multiple DOF as well as thinner than previous research.

Methods

The forceps design was devised to satisfy the requirements of size and maneuverability according to the pediatric surgeons' opinions. Considering the limited workspace of pediatric surgery, the diameter of forceps should be less than 3.5 mm. Moreover, the range of movement should be 60° for opening and closing grasp, $\pm 90^\circ$ for head flexion, and $\pm 180^\circ$ for head rotation.

To achieve the requirements, we suggest the triple-bevel-gear mechanism as shown in Fig. 1(a). This mechanism consists of three types of bevel gear to operate grasping, head flexion, and head rotation. These sets of gears are piled concentrically and tripled. In particular, this mechanism enables forceps to perform grasping or rotating head, while forceps is bended. In addition, this mechanism is able to fit in 3.5 mm in diameter. The advantage of this mechanism is that the pathway of power transmission is almost constant with the forceps posture, compared with wire driving mechanism. However, this mechanism also has disadvantage: the difference between the input and the output caused by gear interference. For example, turning the head flexion gear only, the forceps does not perform the movement of head flexion but the movement of grasp, head flexion, and head rotation.

To resolve the disadvantage of proposed forceps, we suggest the double-headed mechanism as shown in Fig. 1(b). This consists of two triple-bevel-gear mechanisms; one is attached to the head of forceps, the other is enlarged and attached to the handle of forceps.

Results

Figure 2 shows the prototype of proposed forceps. The bevel gears on the forceps head have special shapes. The diameter of the forceps is 3.5 mm. Operating the developed forceps, we checked the ranges of each DOF's movements. The results show 60° for opening and closing grasp, $\pm 90^\circ$ for head flexion, and unlimited head rotation.

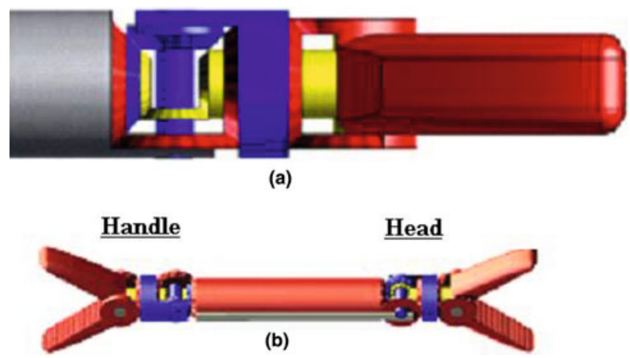

Fig. 1 (**a**) Basic concept of triple bevel gear mechanism, (**b**) Basic concept of double head mechanism

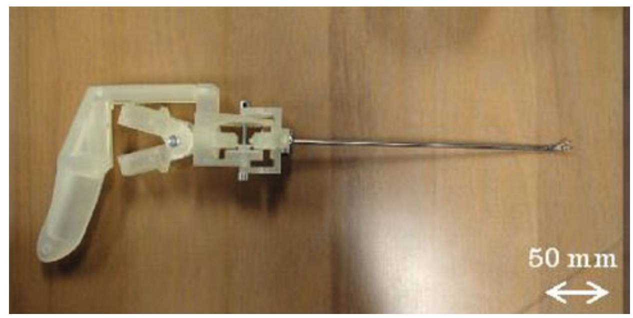

Fig. 2 Overview of developed forceps

Conclusion

This paper proposed and implemented a three-DOF and 3.5-millimeter-diameter forceps for pediatric laparoscopic surgery with the triple-bevel-gear mechanism and the double-headed mechanism. The experiment showed that this forceps fulfills the requirements of pediatric surgeons' opinions. In future, we will improve this forceps in order to apply to the master-slave robotic system for laparoscopic surgery.

Development of an integrated information display system and training system for endoscopic surgical robot system for abdominal surgery

[1]A. Hattori, N. Suzuki, K. Tanoue, S. Ieiri, K. Konishi, H. Kenmotsu, M. Hashizume

[1]The Jikei Univ. School of Medicine, Institute for High Dimensional Medical Imaging, Tokyo, Japan

[2]Kyushu University Hospital, Dept of Advanced Medicine and Innovative Technology, Fukuoka, Japan

[3]Graduate School of Medical Sciences, Kyushu University, Dept of Future Medicine and Innovative Medical Information, Fukuoka, Japan

Keywords Image-guided surgery · Augmented reality · Surgery simulation · Deformable organ model · Surgery training

Purpose

We are in the process of developing an endoscopic surgical robot system for abdominal surgery in our intelligent surgical instruments project [1]. In this system, an operator will operate 2 manipulators which is the robot's arms that is orally injected into a patient's abdominal cavity. The operator in the cockpit will not only see in the display of the operation, navigation function of multi-layered 3D image of patient's X-ray CT and MRI taken before the operation, in real-time, but also various other information necessary for the operator. These information will be displayed around the images of the on-going operation. We are mounting these functions so that we can build an integrated information display system that will enable safer operation for the operator.

We are also developing a training system that can conduct simulation of the operation with the same interface as the actual equipment. In many cases, endoscopic surgical robot system operations in the stomach and digestive organ differ from other existing endoscopic treatment. Therefore we aim to construct a training system that can conduct real-time simulation in a near reality environment and have the operator acquire skills quickly before the system is actually used in clinical practice.

Methods

Integrated information display system: The system has the following five functions. All information is updated in real-time and displayed on the screen in the cockpit for the operator. (1) function that displays the present orientation of the robot by showing patient's X-ray CT and MRI data sets superimposed onto the operation screen, (2) function that displays the position of the tip of the robot on a inner structure model reconstructed in 3D from the patient's X-ray CT and MRI data sets, (3) function that displays the present position of the tip of the robot on patient's X-ray CT and MRI data set images, (4) function that displays the softness of an object that the robot's manipulator has grabbed (this is being developed in parallel with the system), (5) function that displays patient's medical information such as heart rate and blood pressure.

Training system: We reconstructed human soft tissue model of a path from the esophagus to the stomach using sphere filled model structure [2]. The sphere filled stomach wall structure calculates the outside force applied to the robot arm in operation and thus calculates the deformation volume of the stomach wall. With this function, the system can display the deformed walls and also the soft tissue model can calculate reaction force from the deformed stomach walls. We endeavored to have the soft tissue react to the grabbing and lifting by the forceps similarly to the robot arm of the actual system.

Results

Integrated information display system: Fig. 1 shows what the system's screen displays in the operator's cockpit in an animal experiment using a pig. In the center of the screen shows function (1) mentioned earlier, at the upper left, function (2), at the upper right, function (3), at the center left, function (5) and in the lower right and left function 4) which displays the softness of the object the 2 robot manipulators grabbed.

Training system: Fig. 2a,b,c shows the operator operating the robot arm and needle knife in collaboration. The operator is grabbing and resecting the mucosa layer in the stomach. Fig. 2d,e,f shows the operator operating 2 robot arms in collaboration. The operator is in the process of taking out a part of the mucosa layer that has been resected.

Conclusion

With this integrated information display system, in addition to navigation functions, we enabled integrated information display for the operator so that he/she can obtain various pre-operation information and operation information that changes in real-time by taking off his/her eyes from the operation as little as possible.

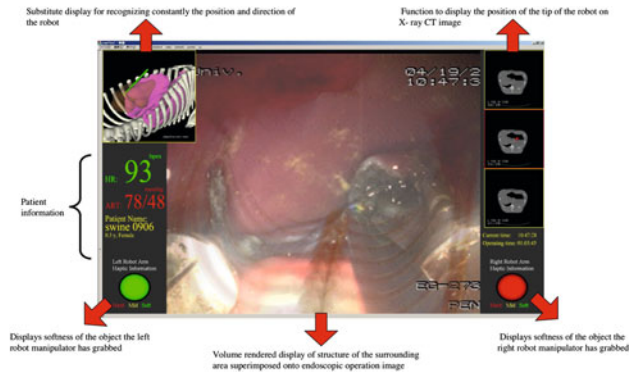

Fig. 1 Integrated information display system screen

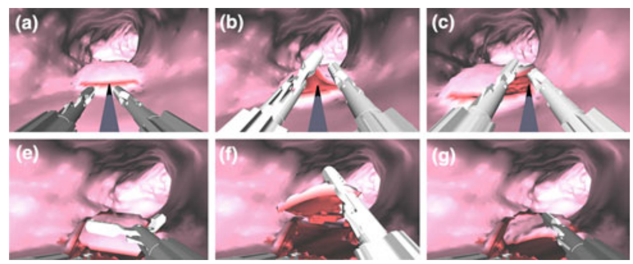

Fig. 2 By grabbing the stomach wall with robot arms, performing dissection of mucosa layer with a needle knife (**a–c**). Dissection of mucosa layer is completed by the collaborative action of 2 robot arms and the mucosa layer that has been cut is being carried out of the body (**d–f**)

Hereafter, we plan to improve the display method of feeding information to the operator based on usage experience. We also plan to sort out information needed by the operator and develop a user interface that will interfere with the operation as little as possible.

For the training system, we plan to mount a function to effectively evaluate the operator by the system. In addition, we plan to make it possible for this training system to be used for trials to design new shape for the robot arm and for trials for new functions.

Acknowledgement

This study was funded by NEDO Intelligent Surgical Instruments Project. (P08006).

References

[1] Suzuki N, Hattori A, Tanoue K, Ieiri S, Konishi K, Kenmotsu H, Hashizume M, Development of endoscopic robot system with augmented reality functions for NOTES that enables activation of four robotic forceps, Proc. of Augmented Medical Imaging including Augmented Reality in Computer-aided Surgery (AMIARCS2009), London

[2] Suzuki S, Suzuki N, Hattori A, Uchiyama A, Kobayashi S, Sphere-filled organ model for virtual surgery system, IEEE Transactions on Medical Imaging, 23(6), 714–22, 2004